Binding of RPE65 Fragments to Lipid Monolayers and Identification of Its Partners by Glutathione *S*-Transferase Pull-Down Assays[†]

Eric Trudel,[‡] Sylvie Beaufils,[§] Anne Renault,[§] Rock Breton,[||] and Christian Salesse*,[‡]

Unité de Recherche en Ophtalmologie and Unité de Recherche en Endocrinologie Moléculaire, Centre de Recherche du CHUQ, Faculté de Médecine, Université Laval, Québec, Québec, Canada G1V 4G2, and Groupe Matière Condensée et Matériaux, UMR-CNRS 6626, Université Rennes 1, 35042 Rennes, France

Received September 26, 2005; Revised Manuscript Received January 19, 2006

ABSTRACT: RPE65 is the major component of the retinal pigment epithelium (RPE) microsomal membrane, and it plays a critical role in the binding of retinoids involved in the visual cycle. To understand how RPE65 binds to membranes, we have expressed and purified soluble fragments of human RPE65 fused to glutathione *S*-transferase (GST). The interaction between two fragments of RPE65 (F1 and F2 which include residues 1−125 and 126−250, respectively) and lipid monolayers has been studied by surface pressure, ellipsometry, and surface rheology measurements. Surface pressure and ellipsometry clearly showed a rapid adsorption of F2 to lipid monolayers whereas the kinetics of binding of F1 was much slower. Furthermore, the data suggest that the F2 fragment inserts into the lipid monolayer. Surface rheology showed a clear increase in monolayer rigidity only in the presence of F2, thereby demonstrating high intermolecular interactions of this fragment. This observation is further supported by the GST pull-down assays which demonstrated that F2 cosediments with full-length RPE65, suggesting that RPE65 has the propensity to form clusters or oligomers. The structure homology modeling of RPE65 based on a related family member, apocarotene 15′,15′-oxygenase, further suggests that a hydrophobic patch located in the F2 region might be responsible for membrane binding. The present work shows that F2 interacts much stronger with lipid monolayers than does F1, which suggests that the region of RPE65 located between residues 126−250 should be very important for its membrane binding. Moreover, given that these fragments are not acylated, these data also suggest that an effective binding of RPE65 to membranes can be achieved without palmitoylation. Furthermore, GST pull-down assays also indicated that F2 interacts with 11-*cis*-retinol dehydrogenase, which supports previous data suggesting that it could act as a partner of RPE65.

Vertebrate phototransduction is initiated by photochemical reaction in which the chromophore of rhodopsin, 11-*cis*-retinal, undergoes isomerization to all-*trans*-retinal (*1*). This isomerization induces the formation of the active form of rhodopsin, metharodopsin II, which decays to yield the aporhodopsin and to finally lead to the release of all-*trans*-retinal (*2*, *3*). The retinoid cycle is an enzymatic cascade taking place both in photoreceptors and in retinal pigment epithelium (RPE),[1] where all-*trans*-retinal is reconverted into 11-*cis*-retinal (*4*−*6*). Two essential reactions occurring in the RPE involve lecithin retinol acyltransferase (LRAT) (*7*, *8*), which produces all-*trans*-retinyl esters, and an isomerase which processes these esters into 11-*cis*-retinol (*9*−*12*). RPE65 was demonstrated to play an essential role in this enzymatic cascade (*13*, *14*). Recently, RPE65 was identified as the isomerase by demonstrating its enzymatic activity in Sf9 cells that express RPE65 (*15*, *16*). Indeed, RPE65 knockout mice are unable to substantially produce 11-*cis*-retinoids, and all-*trans*-retinyl esters were found to accumulate in the RPE of these mice (*17*).

RPE65 is the major component of the RPE microsomal membranes, and it demonstrates high affinity for phospholipids (*18*). The fact that no transmembrane region can be deduced from its primary sequence suggests that RPE65 is a peripheral membrane protein rather than an integral membrane protein (*18*, *19*). The way RPE65 interacts and binds membranes is not well understood. Recently, mass spectrometry studies have shown that RPE65 exists in two forms, a cytosolic form and a membrane-associated form containing three palmitoylations (*20*). It is unclear whether these palmitoylations are required for membrane binding or localization of RPE65 to the microsomal membranes.

In the present study, we have expressed and purified two soluble fragments of RPE65 in fusion with glutathione *S*-transferase (GST) since the full-length RPE65 is not soluble when expressed in *Escherichia coli* and only slightly soluble when expressed in insect cells infected with recombinant

[†] Supported by the Natural Sciences and Engineering Research Council of Canada. E.T. is the recipient of a studentship from the Canadian Institutes of Health Research. C.S. is a Chercheur boursier national from the Fonds de recherche en santé du Québec (FRSQ). The Banque d'Yeux Nationale is partly supported by the Réseau de Recherche en Santé de la Vision.

* Address correspondence to this author. Tel: (418) 656-4141 ext 47243. Fax: (418) 654-2131. E-mail: christian.salesse@crchul.ulaval.ca.

[‡] Unité de Recherche en Ophtalmologie, Université Laval.

[§] Université de Rennes 1.

[||] Unité de Recherche en Endocrinologie Moléculaire, Université Laval.

[1] Abbreviations: RPE, retinal pigmentary epithelium; LRAT, lecithin retinol acyltransferase; IMH, isomerohydrolase; GST, glutathione *S*-transferase; ACO, apocarotenoid 15′,15′-oxygenase.

10.1021/bi0519405 CCC: $33.50
Published on Web 02/14/2006

baculovirus. These fragments were thus used for membrane binding experiments using lipid monolayers at the air−water interface as membrane models. The ellipsometric measurements allowed to show that one fragment strongly binds to phospholipid monolayers. Recent structure determination of the apocarotenoid 15′,15′-oxygenase (ACO) (*21*), a sequence homologue protein showing 25% identity with RPE65, allowed us to generate a RPE65 structure homology model. This model highlights a hydrophobic patch located in a region as a putative membrane binding fragment of RPE65. Moreover, surface rheology with this fragment demonstrated a clear increase in monolayer rigidity, suggesting that RPE65 has the propensity to form oligomers or clusters in membranes. Furthermore, the GST pull-down experiments allowed us to identify a partner of this RPE65 fragment, 11-*cis*-retinol dehydrogenase (11RDH), an enzyme involved in the retinoid cycle.

EXPERIMENTAL PROCEDURES

Expression of Human GST Fusion Fragments of RPE65 in E. coli. RPE65 cDNA was obtained by RT-PCR from human RPE cell mRNA. The full-length RPE65 sequence (GenBank accession number U18991) (*22*) was blunt end ligated into a subcloning vector (pUC19; Fermentas) using the *Sma*I site. The sequences of three different fragments (F1, F2, and F3) of RPE65 were amplified by PCR using the following primers: F1, sense, ATATGAATTCCCTCTATCCAGGTTGAGCATCCT, and antisense, ATCCGCGGCCGCTCATCCTCGAAAGTAAGAAAAAAA; F2, sense, GTAAGAATTCCCGTAGAGGTTACTGACAATGCC, and antisense, AGTAGCGGCCGCTCAGATATAGTTGGGAGTCAGACC; F3, sense, AATGGAATTCCCGTTTTTGTGGAGACACCAGTC, and antisense, TTCCGCGGCCGCTCAAGATTTTTTGAACAGTCCATG. Each fragment has been ligated into pGEX-4T-2 (Amersham) digested with *Eco*RI and *Not*I endonucleases. The reading frame and sequence of the insert were confirmed by automated sequencing. The resulting pGEX-4-T2 clones, in fusion with the C-terminal end of GST, are encoding residues 1−125 for F1, 126−250 for F2, and 251−533 for F3. The estimated expected molecular mass of fusion constructs are 40 kDa for both F1 and F2 and 57 kDa for F3. Expression of the fragments was performed as followed: A single colony of DH-5α transformed with the plasmid of interest was grown overnight in 5 mL of 2× YT (yeast−tryptone) medium containing 100 μg/mL ampicillin. Overnight cultures were diluted 1:100 to inoculate a large-scale culture, which was then induced with 0.1 mM IPTG at $OD_{600} = 0.8$. After induction, bacteria were grown at 37 °C for 3 h, pelleted, and frozen at −80 °C. The majority of protein expression was found as inclusion bodies. The solubilization and purification procedure was adapted from Frangioni et al. (*23*). Briefly, 100 mL culture pellets were resuspended in 20 mL of STE (10 mM Tris, pH 8.5, 150 mM NaCl, 1 mM EDTA), incubated on ice with 100 μg/mL lysozyme, and then adjusted to 5 mM DTT. Bacteria were lysed with the addition of 1.5% sarkosyl (Sigma), sonicated, and clarified at 15000*g* (30 min, 4 °C). Supernatants were adjusted to 2% Triton (Fischer) and applied on a 5 mL GSTrap HP column (Amersham Biosciences). Following column wash with 50 mL of STE and 10 mL of ST (10 mM Tris, pH 8.5, 150 mM NaCl), proteins were eluted with 40 mM glutathione in ST buffer. The estimated purity on gel was about 95% for RPE65 fragments. The yield of purified protein for F1 and F2 is 1.5 and 2 mg/L of bacterial culture, respectively. For membrane binding studies, RPE65 fragments were dialyzed against 5 mM Hepes, pH 7.5, containing 100 mM NaCl. Protein concentration was determined by the BCA method (Bio-Rad). Recombinant GST was purchased from Amersham Bioscience.

Ellipsometric and Surface Pressure Measurements. The ellipsometric measurements were carried out with a null ellipsometer described elsewhere (*24*). The variation of the ellipsometric angle (δ) is a relevant probe of changes occurring at the interface. Basically, δ is related to the phase difference between vertical and horizontal beam polarizations and proportional to the amount of protein adsorbed at the interface. Surface pressure π was measured using a Wilhelmy balance, simultaneously with the measurements of δ with an accuracy of ±0.5 mN/m and ±0.5° for π and δ, respectively. The circular Teflon sample cell has a diameter of 48 mm and a subphase volume of 8 mL. An automated device, using a motor-driven syringe, accounts for the water evaporation by automatically injecting water to the sample cell to maintain a constant subphase level. All experiments were carried out at 20 °C. Lipid monolayers were formed by spreading a known volume of dioleoylphosphatidylcholine (DOPC) (Avanti Polar Lipids) at the air−buffer interface from a 0.5 mM chloroform solution using a gastight syringe until the desired surface pressure of 10 mN/m is reached. Solvent is then allowed to evaporate for approximately 15 min. Initial time points of all graphs ($t = 0$) correspond to the first measurements, once the surface is stable. The zwiterionic DOPC has been used so as to optimize the putative binding of RPE65 fragments by avoiding the effect of lipid polar head charges on monolayer binding. Protein solution can be injected through a hole performed in the sample cell, to a final protein concentration of 15 μg/mL. The buffer used as subphase was 5 mM Hepes (pH 7.5) with 100 mM NaCl. The specific resistivity of ultrapure water used to prepare aqueous solutions was 18×10^6 Ω·cm (Milli-Q; Millipore, Bedford, MA).

Surface Rheology. The rheometer setup and the procedure for data collection and analysis have been previously described (*25*). Briefly, this rheometer uses the action of a very light float (32 mg), which applies a rotational strain to the monolayer through a magnetic torque (with a pair of Helmholtz coils and a small magnetized pin deposited on top of the float). The float is a 10 mm diameter paraffin-coated aluminum disk deposited at the air−water interface. The DOPC monolayer is then spread as described above, and the rigidity is measured. The protein sample is then injected into the subphase, and the rigidity is measured. The Teflon sample cell used for these measurements is the same as that described above. The float carrying a small magnet is kept centered by a permanent field, $B_0 = 6 \times 10^{-5}$ T, parallel to the earth's field which is created by a little solenoid located just above the float. Sensitive angular rotation of the float is achieved by using a mirror fixed on the magnet to reflect a laser beam onto a differential photodiode. A sinusoidal torque excitation is applied to the float in the 0.001−100 Hz frequency range by an oscillating field perpendicular to the permanent solenoid field. The latter field acts as a restoring torque equivalent to a monolayer

with a rigidity of 0.16 mN/m. This number sets the sensitivity of the rheometer. The data presented here provide information on the shear elastic constant or surface rigidity, μ (mN/m), as a function of time. Reproducibility for surface rheology measurements is better than 2 mN/m for surface adsorption kinetics. Initial time points of all graphs ($t = 0$) correspond to the first measurements, once the magnetic float is centered and stable. All experiments were carried out at 20 °C.

RPE Microsomal Membrane Preparation and GST Pull-Down Experiments. Human microsomal membrane extracts from cultured RPE cells were prepared as previously described (*26*). Cultured RPE cells were pelleted by centrifugation at 200*g* for 5 min. The freshly cultured RPE cells were resuspended in TBS (Tris-buffered saline, pH 7.4) containing 2 mM phenylmethanesulfonyl fluoride and homogenized in a Dounce homogenizer on ice. Debris and unbroken cells were removed by centrifugation at 3000*g* for 15 min. The microsomes present in the supernatant were collected by centrifugation at 100000*g* for 1 h. The pellets were flash-frozen in liquid nitrogen and stored at −80 °C. Prior to the binding experiments, the 100000*g* pellets were thawed and suspended in 20 mM Tris, pH 7.5, containing 150 mM NaCl, 1 mM $CaC1_2$, and a protease inhibitor cocktail (Sigma) to a final concentration of 1−2 mg of total protein/mL. The membrane suspension was subsequently passed 10 times through a 22 gauge needle and finally sonicated with 10 pulses (1 s) using a microprobe. All steps were performed on ice or at 4 °C.

The microsomal membrane extract is then added to immobilized GST-fused RPE65 fragments on glutathione−Sepharose 4B beads (Amersham Biosciences). A control experiment with GST alone has also been performed. After 2 h incubation at 4 °C, the beads were washed extensively with pull-down buffer (20 mM Tris, pH 7.4, 100 mM NaCl, 1 mM $CaCl_2$) by centrifugation at 500*g*, and bound proteins were eluted with SDS−PAGE loading buffer and separated on 12% (w/v) SDS−polyacrylamide gels. Following electrophoresis, gels were analyzed either by Coomassie staining or by western blot. For the latter, gels were blotted onto PVDF membranes (Millipore Corp., Bedford, MA). Blots were incubated with 5% (w/v) nonfat dried milk (NFDM) in TBS-T [TBS containing 0.2% (v/v) Tween-20]. Immunoblots were incubated overnight at 4 °C with mouse anti-RPE65 (1:5000) antibody (kindly provided by Dr. D. Thompson) in 1% (w/v) NFDM in TBS-T. After washing, immunoblots were incubated at 20 °C with the secondary antibody [sheep anti-mouse IgG peroxidase (Sigma Chemical Co., St. Louis, MO)] (1:2000) in TBS-T. Immunoblots were analyzed using a Gel doc imaging system (Bio-Rad).

Protein Identification by LCMS/MS. SDS−PAGE gel bands were excised and digested with porcine trypsin (6 ng/μL) for 5 h on a MassPrep robotic workstation (Micromass). Peptides were extracted in a final volume of 45 μL of 0.5% formic acid (v/v) and 9% acetonitrile (v/v). Tryptic peptides were analyzed on a QTrap 4000 ion trap mass spectrometer (Applied Biosystems). Briefly, the sample was applied to a 10 cm × 75 μm Pico Frit column containing BioBasic C18 packing. Peptides were eluted from the column using a 10−95% acetonitrile (v/v) gradient containing 0.1% formic acid (v/v) at a flow rate of 200 nL/min. Eluted peptides were electrosprayed as they exited the column, and doubly, triply, or quadruply charged ions were selected for passage into a collision cell. Fragmentation was facilitated by collision with nitrogen gas, and data were collected. Three scans at a speed of 4000 amu/s from *m*/*z* 50 to *m*/*z* 1700 were averaged. Peak lists of MS/MS data were prepared using a Mascot peak list generating script on BioAnalyst 1.4 software (Applied Biosystems) and submitted to Mascot (Matrix Science) for identification by analysis against the NCBI nonredundant database with a 1.5 Da resolution.

RPE65 Structure Homology Modeling. The homology model of RPE65 was built on the basis of coordinates from the crystal structure of ACO (PDB ID 2BIW) (*21*) using the CPHmodels program (*27*). Protein sequence alignments were performed using the CLUSTALW program with amino acid classes described by Bork et al. (*14*). Alignments of three-dimensional structures and structural analyses were performed using UCSF Chimera (*28*). Images depicting solvent-excluded molecular surfaces were created with the MSMS package (*29*).

RESULTS

Production of Soluble GST-Fused Fragments of RPE65. In our experiments as well as those reported by others (*30*), the full-length RPE65 is not soluble when expressed in *E. coli* whereas a high yield of expression is obtained with the baculovirus expression system in insect cells. However, most of the expressed RPE65 in infected insect cells can be found in inclusion bodies such that only a very small fraction of RPE65 is soluble, which prevents its use for membrane binding or structural studies. However, in the presence of detergent, the use of the baculovirus expression system in insect cells allowed to obtain enough RPE65 to demonstrate retinoid binding properties since only a small amount of protein is necessary to perform such spectroscopic measurements (*31*, *32*).

Given that RPE65 is a highly insoluble protein, we have chosen to express GST fusion fragments of this protein. The GST fusion protein system is a widely used recombinant protein expression system that allows easy purification but, more importantly in our experiments, a potential increase in overall solubility of the fused protein (*33*). It is noteworthy to mention that the fusion protein of the full-length RPE65 with GST was expressed as insoluble inclusion bodies. Thus, GST-fused fragments of RPE65 were expressed to obtain soluble portions of the protein. Since there is no structural information on RPE65, or any known functional domains of the protein, many criteria were considered in order to express potential domains or motifs of RPE65. Using the Kyte and Doolittle hydropathy index profile (*34*) with the amino acid sequence of human RPE65, no significant hydrophobic stretches of amino acids can be found, which could explain the low solubility of RPE65 or its interaction with membranes. Furthermore, no consensus was obtained when using the available structure prediction softwares to identify hydrophobic regions in RPE65 or any secondary structural features (GOR, DAS, PSIPRED, SSPRO) (*35*−*38*). Sequence alignments of RPE65 from different species do not provide any insight on the possible formation of domains since the sequence identities from human to salamander RPE65 are more than 85% (*39*). However, the alignment with other family members of RPE65, such as

β-carotene dioxygenase and ACO (*21*), shows variable short sequences. On the basis of these observations, several constructs of RPE65 were designed. Among these constructs, two fragments of RPE65, expressed as GST fusion proteins, were soluble after purification. These are fragments 1 (F1) and 2 (F2) comprising residues 1−125 and 126−250, respectively.

F1 and F2 were expressed as inclusion bodies, which were soluble with 1% sarkosyl, an anionic detergent often used for the solubilization of inclusion bodies of GST fusion proteins (*23*, *40*). In addition, they remain soluble after sarkosyl elimination with buffer exchange on the affinity column. However, cleavage of the GST fusion partner of F1 and F2 with thrombin protease rapidly caused their aggregation, even at low protein concentration (<0.5 mg/mL). This aggregation further demonstrates the insoluble nature of RPE65. One could thus postulate that membranes correspond to a more favorable environment for RPE65. Membrane binding studies were thus performed with GST fusion fragments since the solubility of F1 and F2 is dramatically increased to approximately 2 and 11 mg/mL, respectively, when fused to GST. Other GST-fused constructs such as the recombinant RPE65, fragment 3 (F3, residues 251−533), and fragment 2−3 (F2−3, residues 126−533) were assayed for their solubility and were found to be expressed as sarkosyl-insoluble inclusion bodies. Solubilization assays of these inclusion bodies have also been performed under denaturating conditions in the presence of guanidine (5 M) or urea (8 M), followed by renaturation by dialysis or rapid dilution (*41*). However, only protein aggregates have been obtained.

Surface Pressure and Ellipsometric Measurements. The adsorption kinetics for F1 and F2 as well as pure GST onto phospholipid monolayers are shown in Figure 1. It can be seen that the adsorption of these protein fragments at the air−water interface in the absence (Figure 1A) and in the presence (Figure 1B) of a DOPC monolayer leads to an increase in surface pressure (π) as a function of time. In the absence of a phospholipid monolayer (Figure 1A), F2 shows a very fast and large extent of adsorption as demonstrated by its kinetics of adsorption and the high surface pressure obtained at saturation (π = 16.2 mN/m) in contrast to F1, which shows a very slow kinetics of adsorption and the small value of surface pressure reached at saturation (π = 1.5 mN/m). The adsorption of GST alone at the air−water interface shows a rapid increase of surface pressure to a value of approximately 7 mN/m at saturation. Given that RPE65 fragments F1 and F2 are in fusion with GST, this tensioactive behavior of GST suggests that it partly contributes to the adsorption behavior of F2 but not that of F1 since the affinity of F1 toward the interface is very low. These data indicate a strong surface activity of F2 whereas that of F1 is much smaller. When these protein fragments are injected underneath a DOPC monolayer (Figure 1B) equilibrated at an initial surface pressure of 10 mN/m, a similar behavior to that observed in the absence of a lipid monolayer can be measured (compare panels A and B of Figure 1). Indeed, a fast and large increase in surface pressure can be observed for F2 and GST, but a very slow increase can be seen for F1. A maximum surface pressure of 28 mN/m has been reached with F2 compared to 19.5 mN/m for GST and 17 mN/m for F1, after 5, 2, and 15 h of kinetics, respectively.

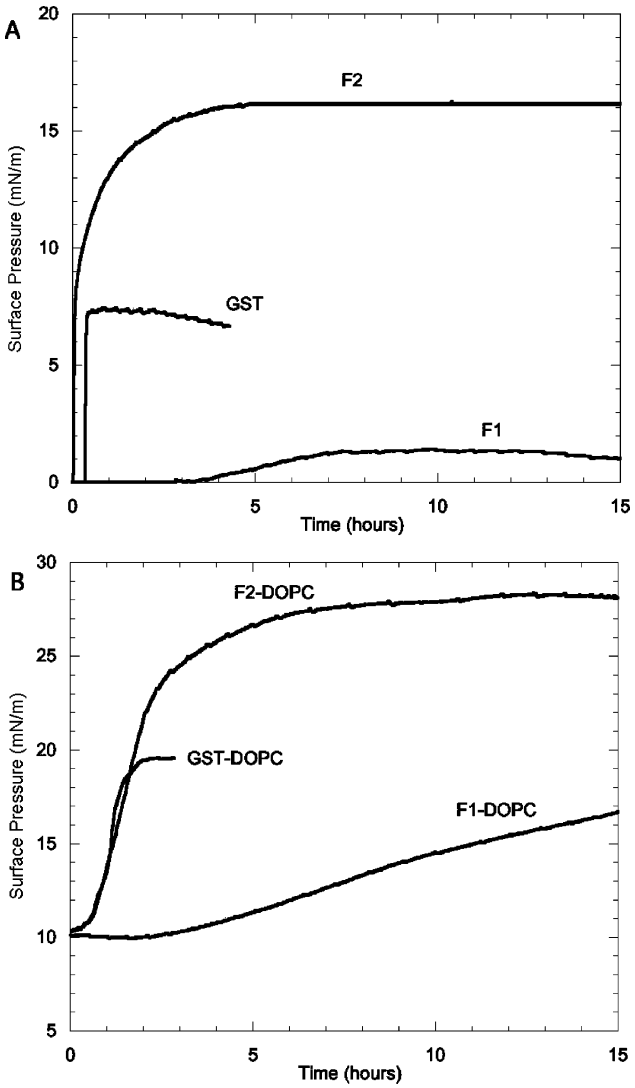

FIGURE 1: Kinetics of adsorption of RPE65 fragments and GST in monolayers at the air−water interface from the measurement of surface pressure. F1, F2, and GST are injected into a subphase containing 5 mM Hepes, pH 8.0, and 100 mM NaCl (A) in the absence (F1, F2, and GST) or (B) in the presence (GST−DOPC, F1−DOPC, and F2−DOPC) of a DOPC monolayer which has been equilibrated at 10 mN/m prior to protein injection. The final protein concentration in the subphase is 15 μg/mL.

The evolution of the ellipsometric angle δ as a function of time upon adsorption of F1, F2, and GST in the presence and in the absence of a DOPC monolayer is presented in Figure 2. In the absence of a DOPC monolayer, ellipsometric angles of 1.2° and 2.2° are reached at saturation after several hours of adsorption of F1 and GST, respectively. In contrast, a much higher ellipsometric angle of 9.5° is obtained much faster (1.5 h) after injection of F2 into the subphase. The same experiments were carried out in the presence of a DOPC monolayer equilibrated at an initial surface pressure of 10 mN/m. The DOPC monolayer contributes to the ellipsometric signal (δ = 2.8°) (see dashed lines in Figure 2). Therefore, the ellipsometric signal upon adsorption of F1, F2, and GST onto the DOPC monolayer starts at an ellipsometric angle δ = 2.8°. The adsorption curve obtained upon injection of GST underneath the DOPC monolayer (Figure 2A) merely corresponds to adding the ellipsometric angle obtained for pure DOPC (δ = 2.8°) to that of pure GST (in the absence of DOPC) as described by $\delta_{GST-DOPC}$

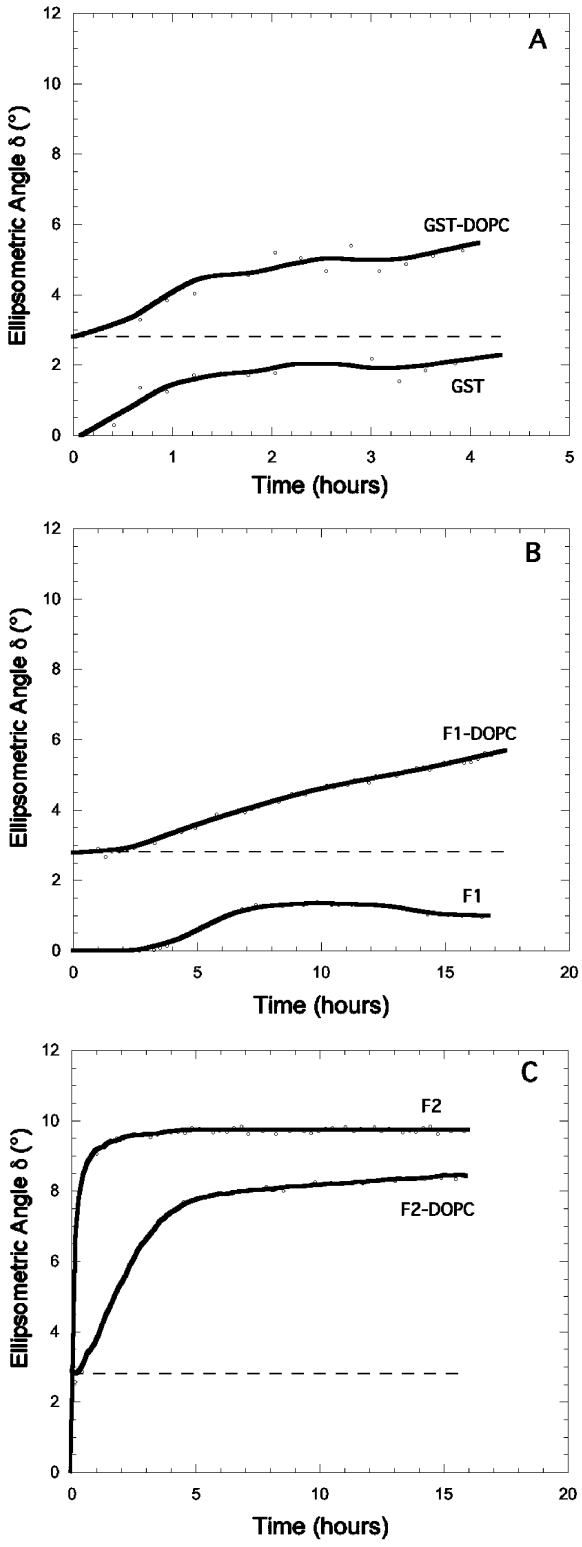

FIGURE 2: Kinetics of adsorption of RPE65 fragments and GST in monolayers at the air−water interface as measured by ellipsometry. Measurement of the ellipsometric angle δ has been performed after the injection of (A) GST, (B) F1, and (C) F2 into the subphase in the absence (F1, F2, and GST) or in the presence (GST−DOPC, F1−DOPC, and F2−DOPC) of a DOPC monolayer. The DOPC monolayer was equilibrated at 10 mN/m prior to protein injection. The ellipsometric angle of DOPC ($\delta = 2.8°$) is shown as a dashed line. Other conditions are the same as described in Figure 1.

$= \delta_{GST} + \delta_{DOPC}$. The ellipsometric signal can be assumed to depend solely on monolayer thickness. Indeed, the measurement of an ellipsometric angle indicates that the interfacial layer has induced a phase change of the polarized light. In the case of a sufficiently dense film, the refractive index of this film is independent of the film thickness. Consequently, the observed phase change of the dense film is proportional to the film thickness. We thus assumed that the pure GST and the mixed GST−DOPC films had reached such a sufficiently high film density close to the end of their respective ellipsometric isotherm. The observation of $\delta_{GST-DOPC} = \delta_{GST} + \delta_{DOPC}$ thus suggests that GST adsorbs at the surface of the DOPC monolayer without penetrating this monolayer. Furthermore, the high similarity between the kinetics of adsorption of GST in the presence and the absence of DOPC suggests that DOPC has no influence on the kinetics of GST adsorption and that GST binds DOPC with very low affinity. Similar observations can be made during the first 7 h of the adsorption kinetics of F1. Indeed, for example at time $t = 6$ h, the sum of the ellipsometric angle of pure DOPC (2.8°) and F1 (1.0°) in the absence of DOPC (Figure 2B) is very similar to the ellipsometric signal obtained when F1 is injected underneath the DOPC monolayer (3.8°), which thus corresponds to $\delta_{F1-DOPC} = \delta_{F1} + \delta_{DOPC}$. These data thus suggest that, as observed with GST, F1 does not penetrate the DOPC monolayer and only weakly interacts with DOPC. However, over a longer period of time (more than 7 h), the ellipsometric angle of the F1−DOPC monolayer is still increasing, whereas that of F1 in the absence of DOPC is already saturated after ~7 h. Although the kinetics of adsorption of F1 in the presence of DOPC (Figure 2B) is very slow compared to F2 (Figure 2C), the difference observed after 7 h between the kinetics of adsorption of F1 in the presence and absence of DOPC suggests that some type of interaction between F1 and DOPC takes place from this point. In contrast, F2 exhibits a completely different behavior. Indeed, a much smaller ellipsometric angle of approximately 5.7° is reached for F2 at saturation [after subtraction of the contribution of pure DOPC (2.8°)] compared to 9.5° in the absence of a DOPC monolayer. This significant decrease of δ in the presence of DOPC suggests that F2 extensively penetrates into the monolayer, rather than being juxtaposed underneath the DOPC monolayer as observed in the case of GST and F1. In fact, when F2 binds to the DOPC monolayer, the resultant ellipsometric signal is smaller than the sum of the ellipsometric signal of the individual F2 and DOPC components: $\delta_{F2-DOPC} < \delta_{F2} + \delta_{DOPC}$. A model of the organization of F1 and F2 at the lipid interface is presented in Figure 7. Overall, these results demonstrate that F2 binds much more extensively to the DOPC monolayer than F1 and GST and that F2 is penetrating into the lipid monolayer, as opposed to F1 and GST.

Surface Rheology Measurements. Although ellipsometric and surface pressure measurements were useful to monitor the adsorption kinetics of the RPE65 fragments onto a lipid monolayer, these methods provide no information on the lateral rigidity of the adsorbed protein. The nonzero shear rigidity, μ, provides information on the lateral organization of proteins in the monolayer plane (*25*). Therefore, we performed surface rheology experiments with F1, F2, and GST to monitor the evolution of rigidity of these monolayers with time (Figure 3). A significant increase in rigidity was only observed with F2, both in the presence and in the absence of the DOPC monolayer. A noticeable increase in μ occurs after the adsorption of F2 for approximately 3 h in

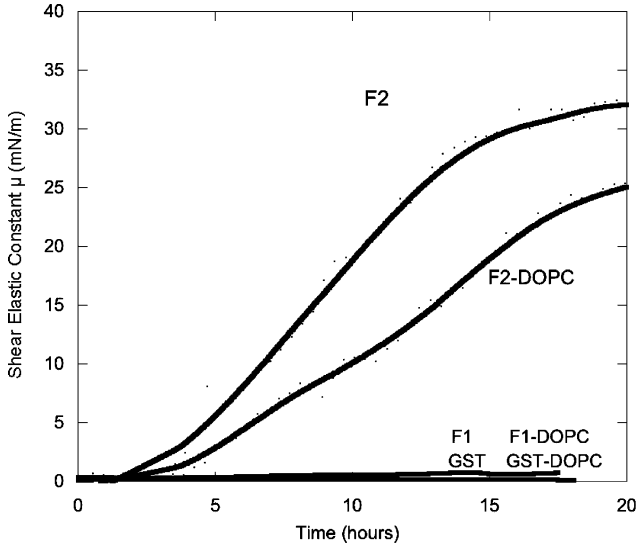

FIGURE 3: Shear elastic constant μ versus time of RPE65 fragments and GST at the air−water interface (F1, F2, and GST) as well as when injected underneath a DOPC monolayer (GST−DOPC, F1−DOPC, and F2−DOPC). Other conditions are the same as described in Figure 1.

the presence and the absence of DOPC, but the kinetics of rigidification is slightly faster in the absence of DOPC. However, the average final rigidity values are not significantly very different ($\mu = 30$ mN/m for F2 alone and $\mu = 26.5$ mN/m for the F2−DOPC monolayer) since the accuracy of these measurements is ~2 mN/m. However, the slower rigidification in the presence of DOPC could be attributed to the lag time required by F2 to reorganize into the fluid DOPC monolayer. These results strongly suggest that intermolecular interactions between F2 proteins take place upon adsorption to the lipid-free surface.

GST Pull-Down Experiments. To investigate possible interactions of F1 and F2 with full-length RPE65 and/or other components of the RPE, we took advantage that our fragments of RPE65 are fused to GST to perform GST pull-down experiments. Fragments of RPE65 (as well as GST as a control experiment) were bound to glutathione−Sepharose and then incubated with a microsomal membrane extract from human RPE cells. After extensive washing of the Sepharose resin, the bound proteins were eluted and separated by electrophoresis. A band at 61 kDa was revealed by Coomassie staining when the Sepharose-immobilized F2 was incubated with the RPE extract (Figure 4A). This band did not appear in controls, which suggests that it binds specifically to F2. A western blot was then performed to identify this protein by using an antibody against RPE65. As can be seen in Figure 4B, the band at 61 kDa is RPE65 comigrated with F2 at 40 kDa, which is also recognized by this antibody. Moreover, RPE65 did not bind to F1 nor to GST, and in contrast to F2, no band on the Coomassie-stained gel could be attributed to binding of a unique protein to F1 or GST when compared to controls (data not shown). This result shows that F2 can bind the full-length RPE65. An additional protein that binds specifically to F2 was observed at 35 kDa by Coomassie staining and was subjected to identification by mass spectrometry after band cutting and digestion with trypsin. The peptides identified by mass mapping with LC/MS-MS (Table 1) correspond to human 11RDH. Altogether, these results strongly suggest that residues 126−250 of

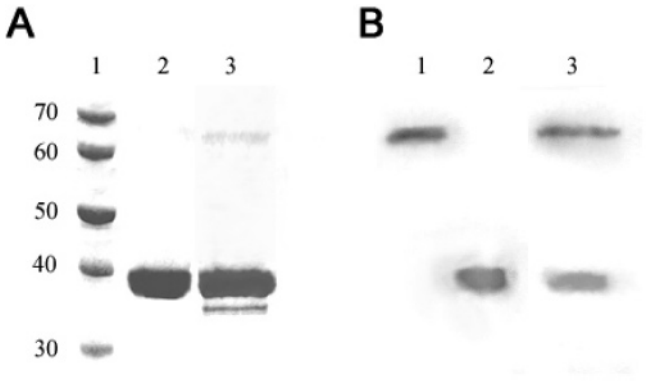

FIGURE 4: GST pull-down assays using immobilized F2. (A) SDS−PAGE Coomassie staining: lane 1, molecular weight standards; lane 2, purified F2 bound to glutathione−Sepharose resin; lane 3, cosedimentation of 11RDH (35 kDa) and RPE65 (65 kDa) to immobilized F2. (B) Immunoblots with anti-RPE65: lane 1, RPE cell extract; lane 2, immobilized F2 bound to glutathione−Sepharose resin; lane 3, cosedimentation of RPE65 with F2.

RPE65 promote the self-association of RPE65 and that this region of RPE65 interacts with 11-RDH, which is also involved in the visual cycle.

RPE65 Structure Homology Modeling. Very recently, the structure of ACO, an enzyme showing 25% identity with RPE65 (Figure 5), was solved by X-ray crystallography (*21*). ACO has been found in plant and cyanobacteria and is responsible for the biosynthesis of pigments, cleaving β-carotene to yield two molecules of retinal. The ACO structure allowed us to create a model for RPE65, based on their sequence identity, and to fit the F1 and F2 fragments within this structural model. The structure calculated predicts that RPE65 is most likely to form a seven-bladed β-propeller (Figure 6A). However, since RPE65 and ACO are 533 and 490 residues long, respectively, many gaps are found within their sequence alignment (Figure 5). This length discrepancy might allow RPE65 to form longer loops interconnecting the propeller's blades, or an eight-bladed β-propeller.

The alignment of RPE65 with ACO (Figure 5) shows a region of RPE65 from residue 118 to residue 125 that is absent in the ACO sequence. Interestingly, this region specific to RPE65 was selected to separate the F1 and F2 fragments. In the ACO crystal structure, this region is located in a loop connecting the first and second blade. On the other hand, the F2 sequence covers blades 2 and 3 of the propeller and forms large loops extending on both sides of the propeller axis.

Further analysis of this RPE65 structural model shows that the four conserved histidines (see Figure 5), responsible for Fe^{2+} coordination, are also pointing toward the inside of the β-propeller. These histidines are also conserved among six members of the carotenoid oxygenase family (*21*). Furthermore, it was recently shown that RPE65 can bind iron (*42*). The correct orientation of these histidines to form a coordination cluster suggests that the backbone of this RPE65 model is appropriately predicted in this region.

Structural analysis of the ACO reveals a hydrophobic patch on the surface of this seven-bladed β-propeller, presumably being responsible for membrane binding (*21*). The nonpolar residues forming this hydrophobic patch are shown in the sequence alignment with RPE65 (see Figure 5). These residues are not well conserved with the RPE65 sequence,

Table 1: Tryptic Peptides of 11RDH Identified by MALDI-TOF

peptide sequence[a]	start−end[b]	monoisotopic mass ([M + H$^+$]) theoretical	experimental
MWLPLLLGALLWAVLWLLR	1−19	2277.24	2276.36
QSLPASNAFVFITGCDSGFGR	22−42	2174.24	2173.03
EAGLFGLVNNAGVAGIIGPTPWLTR	102−126	2521.76	2522.36
VLNVNTMGPIGVTLALLPLLQQAR	132−155	2531.36	2530.47
VINITSVLGR	158−167	1071.11	1070.64
LAANGGGYCVSK	168−179	1139.31	1138.54
FGLEAFSDSLR	180−190	1241.57	1240.61
TPVTNLESLEK	210−220	1228.87	1229.65
TLQACWAR	221−228	948.31	947.46
LPPATQAHYGGAFLTK	229−244	1671.74	1670.88
CLEHALTAR	267−275	1011.78	1012.51
YSPGWDAK	281−288	923.23	922.42

[a] Amino acid residues derived from the 38 kDa protein. [b] Position of the amino acid residue in the deduced peptide sequence of human 11RDH.

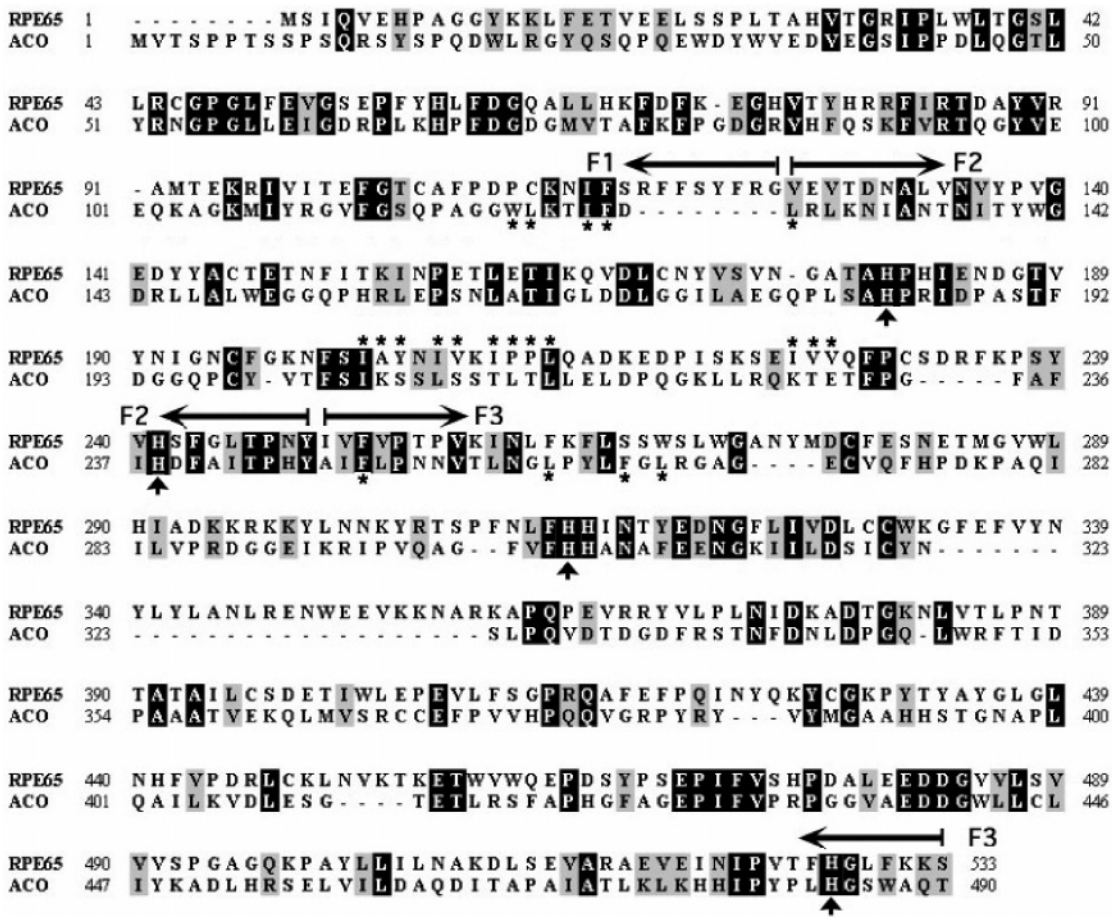

FIGURE 5: Sequence alignment of RPE65 and ACO. Identical residues are shaded in black whereas those showing similarity acording to the Blosum 62 matrix are shaded in gray. The four conserved histidines are shown by arrows under the sequence. The residues responsible for the hydrophobic patch are marked with an asterisk (see above the sequence of RPE65 and under the sequence of ACO. Arrows under the sequence show the limits of fragments F1, F2, and F3.

suggesting that this nonpolar patch is not located in this region for RPE65. However, our model shows a hydrophobic patch at the surface of RPE65 (Figure 6B) which is located within a region of F2. This patch is composed of residues poorly conserved within the ACO sequence, suggesting the nonpolar patches are not located at the same position in RPE65 and ACO structures.

DISCUSSION

As reported in the present study and observed by other investigators (*30*), RPE65 was found to be insoluble when expressed in *E. coli*. On the other hand, expression in insect cells produces very small amounts of soluble RPE65, and only very low concentrations of soluble protein can be obtained with detergent. Moreover, although RPE65 has been shown to be closely associated with membranes (*18*), no transmembrane domain has been identified on the basis of its primary structure (*26*). The protein segment of RPE65 responsible for this interaction is thus still unknown. The study of different fragments of RPE65 is thus important to dissect the functional and structural features of this protein. Several fragments of RPE65 have thus been expressed to

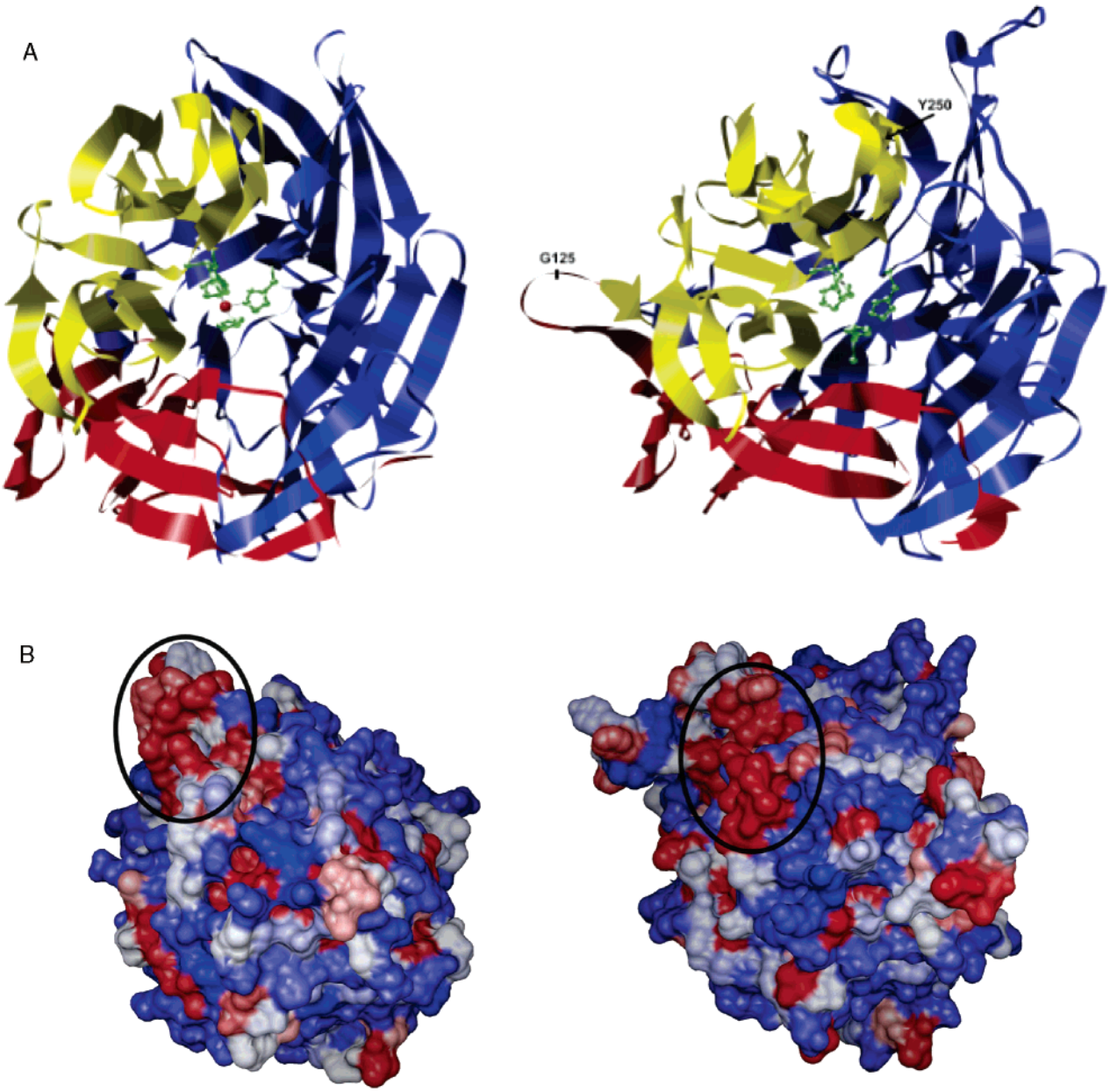

FIGURE 6: Structure of ACO and the homology model of RPE65 based on the structure of ACO (PDB ID 2BIW) which are shown in the same orientation according to their structural alignment. (A) Ribbon plot of the ACO (left) and RPE65 (right) chain fold. The view is perpendicular to the axis propeller, showing in both structures the four iron binding histidines. Chains are colored with reference to the three fragments F1, F2, and F3 in yellow, red, and blue, respectively. (B) Surface representation of ACO (left) and RPE65 (right) color coded according to the hydropathy index of their residues. The nonpolar patch is circled in both structures at different locations.

enable such membrane binding studies to clarify this issue. Moreover, these fragments were also used to identify binding partners of RPE65 that could be involved in the visual cycle to regenerate 11-*cis*-retinal. These RPE65 fragments were expressed as GST fusion proteins. In fact, the presence of GST is essential for their solubility in the absence of detergent. Indeed, the cleavage of this fusion protein readily yields protein aggregation. It is still, however, unclear why the C-terminal region of RPE65 cannot be solubilized, whether it is expressed as misfolded protein or whether it is due to the presence of an additional hydrophobic region of RPE65.

Phosphatidylcholine (PC) is one of the major phospholipids of RPE cell membranes (*43*). Moreover, a greater cosedimentation of RPE65 has been previously observed with PC than PS (phosphatidylserine) containing liposomes (*18*). In addition, to observe hydrophobic driven binding of RPE65 to membranes, it is preferable to use a zwiterionic phospholipid like phosphatidylcholine to reduce the effect of charges on monolayer binding. DOPC monolayers were thus used as model membranes to optimize the putative binding of RPE65 fragments. Furthermore, an initial DOPC monolayer surface pressure of 10 mN/m has been used to allow observation of a large surface pressure increase that can be properly analyzed upon adsorption of RPE65 fragments.

The ellipsometric and surface pressure data consistently showed a fast and strong binding of F2 to DOPC monolayers with a larger surface coverage than F1 or GST. Furthermore, the smaller ellipsometric angle obtained with F2 in the presence than in the absence of the DOPC monolayer suggests that F2 penetrates into the lipid monolayer whereas F1 or GST are probably only loosely bound at the interface

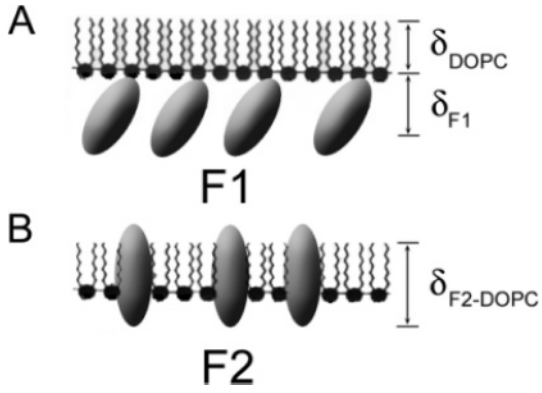

FIGURE 7: Schematic diagram of the possible organization of F1 and F2 fragments interacting with the DOPC monolayer. When F2 binds to the DOPC monolayer, the resultant ellipsometric signal is smaller than the sum of the ellipsometric signal of the individual F2 and DOPC components: $\delta_{F2-DOPC} < \delta_{F2} + \delta_{DOPC}$. As observed with GST, F1 does not penetrate the DOPC monolayer and only weakly interacts with DOPC, which thus corresponds to $\delta_{F1-DOPC} = \delta_{F1} + \delta_{DOPC}$.

of the DOPC monolayer. This strong membrane binding of RPE65 should favor its interactions with partners such as 11RDH which is membrane embedded.

A large number of proteins have been shown to interact with lipid monolayers. However, to our knowledge, only amyloid precursor protein (*44*, *45*) and calcineurin (*46*) have been shown to increase monolayer surface pressure as much as F2 (from 10 to 28 mN/m). Indeed, the 116 kDa amyloid precursor protein and the 77 kDa calcineurin have also been shown to display high surface activity. When injected underneath a DOPC monolayer at 10 mN/m, surface pressures at saturation of 27 and 24 mN/m have been measured respectively for the amyloid precursor protein and calcineurin. As in the case with F2, the insertion of these proteins into the lipid monolayer has been postulated to be mediated by hydrophobic interactions.

Previous studies have shown that cytosolic and palmitoylated forms of RPE65 can be found in bovine RPE cells (*30*). The cytosolic form is often referred to as the soluble RPE65 (sRPE65) although it also requires detergent for its solubilization, like its membrane-bound counterpart (mRPE65). Bavik and co-workers (*13*) have noticed that both forms of RPE65 are extracted in the detergent phase of Triton X-114, suggesting the presence of extensive hydrophobic regions in the protein. The present results agree well with these observations since our F1 and F2 fragments precipitate when the GST fusion protein is removed. This is also consistent with the observation of F2 penetration into the DOPC monolayer, which suggests that a region of RPE65 located between residues 126 and 250 is highly hydrophobic. This ability of F2 to penetrate membranes must be accounted for solely by protein hydrophobic interactions because RPE65 fragments cannot be acylated when expressed in *E. coli* in our experiments. From the RPE65 model structure, this binding can be attributed to a hydrophobic patch on the surface and not to a transmembrane portion of the protein (see Figure 6B). This patch located on the F2 fragment might be responsible for the rapid membrane binding observed in the lipid monolayer studies (Figure 6B). The β-propeller fold has been found and predicted in many different structures and is accomplishing a variety of functions (*47*). Despite the fact that β-propeller folds share low sequence similarity and frequently show no easily detectable sequence repeats, such as in the case of RPE65 and ACO, their three-dimensional structures and their individual blades are very closely superimposable (*48*−*50*). Their functions are specified by the characteristics of their surface and interconnecting loops.

RPE65 was shown to bind long-chain hydrophobic all-*trans*-retinyl esters (*31*). Given that retinyl esters are very hydrophobic molecules which must either be associated with membranes or be bound to proteins, the strong anchoring of RPE65 to membranes through its F2 region could allow it to achieve retinoid binding. Moreover, it has been suggested that the reversible interconversion of sRPE65 to mRPE65 catalyzed by LRAT could account for a putative regulation of RPE65 function (*20*). The palmitoylation sites are located at the end of F2 (C231) and outside of F2 (C329 and C330). However, it was recently shown that C330Y-substituted RPE65 leads to the complete loss of isomerase activity, suggesting that residue C330 may play a role beyond modulating the affinity of RPE65 for membranes (*15*). It could thus be postulated that palmitoylations of the membrane-bound RPE65 could possibly serve to modulate the extent of its membrane binding, which would allow it to achieve a more efficient release or binding of retinyl esters. On the other hand, these acylations might not be the main contribution to RPE65 membrane binding characteristics.

The large surface rigidity observed with F2 is typically taking place when protein−protein interactions occur, such as in the case of the polymerization of actin (*51*) or the dimerization of β-lactoglobulin (*52*). Therefore, although the detailed organization of F2 bound to lipid monolayers is unknown, it must be organized such that intermolecular interactions are highly favored. This high rigidity of F2 could be attributed to the formation of dimers. However, the GST fusion partner of F2 is known to dimerize individually as well as in fusion with other proteins and could thus be responsible for this observation (*53*−*56*). This possibility is, however, unlikely on the basis of the GST pull-down experiments which showed that F2 interacts with full-length RPE65 extracted from RPE microsomal membranes and which thus is not a GST fusion protein. This F2−RPE65 interaction together with the observed large rigidity of F2 thus suggests that a structural feature of F2 could favor the oligomerization or clustering of RPE65 to enable its function.

The GST pull-down assays strongly suggest that RPE65 also interacts with 11RDH, which is involved in the conversion of 11-*cis*-retinol to 11-*cis*-retinal (*57*). Similarly to RPE65, 11RDH is involved in the visual cycle and is membrane associated (*58*). Simon and co-workers (*59*) previously observed a direct protein−protein interaction between RPE65 and 11RDH while attempting to purify 11RDH using specific antibodies for this protein (*60*). In the present work, we also demonstrate that F2 binds 11RDH. In addition, we localized the RPE65 binding region to 11RDH within residues 126−250. However, which region of 11RDH is involved in this interaction is still unknown. Since the ellipsometric results suggest that F2 is inserted into phospholipid membrane, it could interact with either of the two transmembrane C-terminal or N-terminal domains of 11RDH, which are both acting as anchors to the microsomal membrane (*61*). Moreover, 11RDH could be used in future

studies to facilitate the solubilization and the crystallization of RPE65.

ACKNOWLEDGMENT

The authors thank Dr. Debra Thompson (Department of Ophthalmology and Visual Sciences, University of Michigan) for a generous gift of anti-RPE65 and the Banque d'Yeux Nationale for providing us with human eyes.

REFERENCES

1. Wald, G. (1968) Molecular basis of visual excitation, *Science 162*, 230−239.
2. Hamm, H. E., and Gilchrist, A. (1996) Heterotrimeric G proteins, *Curr. Opin. Cell Biol. 8*, 189−196.
3. Hamm, H. E. (1998) The many faces of G protein signaling, *J. Biol. Chem. 273*, 669−672.
4. McBee, J. K., Palczewski, K., Baehr, W., and Pepperberg, D. R. (2001) Confronting complexity: the interlink of phototransduction and retinoid metabolism in the vertebrate retina, *Prog. Retinal Eye Res. 20*, 469−529.
5. Rando, R. R. (2001) The biochemistry of the visual cycle, *Chem. Rev. 101*, 1881−1896.
6. Kuksa, V., Imanishi, Y., Batten, M., Palczewski, K., and Moise, A. R. (2003) Retinoid cycle in the vertebrate retina: experimental approaches and mechanisms of isomerization, *Vision Res. 43*, 2959−2981.
7. Barry, R. J., Canada, F. J., and Rando, R. R. (1989) Solubilization and partial purification of retinyl ester synthetase and retinoid isomerase from bovine ocular pigment epithelium, *J. Biol. Chem. 264*, 9231−9238.
8. Saari, J. C. (2000) Biochemistry of visual pigment regeneration: the Friedenwald lecture, *Invest. Ophthalmol. Visual Sci. 41*, 337−348.
9. Deigner, P. S., Law, W. C., Canada, F. J., and Rando, R. R. (1989) Membranes as the energy source in the endergonic transformation of vitamin A to 11-cis-retinol, *Science 244*, 968−971.
10. Bok, D. (2004) Gene therapy of retinal dystrophies: achievements, challenges and prospects, *Novartis Found. Symp. 255*, 4−12 (discussion 12−16, 177−178).
11. Gollapalli, D. R., Maiti, P., and Rando, R. R. (2003) RPE65 operates in the vertebrate visual cycle by stereospecifically binding all-trans-retinyl esters, *Biochemistry 42*, 11824−11830.
12. Moiseyev, G., Crouch, R. K., Goletz, P., Oatis, J., Jr., Redmond, T. M., and Ma, J. X. (2003) Retinyl esters are the substrate for isomerohydrolase, *Biochemistry 42*, 2229−2238.
13. Bavik, C. O., Levy, F., Hellman, U., Wernstedt, C., and Eriksson, U. (1993) The retinal pigment epithelial membrane receptor for plasma retinol-binding protein. Isolation and cDNA cloning of the 63-kDa protein, *J. Biol. Chem. 268*, 20540−20546.
14. Hamel, C. P., Tsilou, E., Pfeffer, B. A., Hooks, J. J., Detrick, B., and Redmond, T. M. (1993) Molecular cloning and expression of RPE65, a novel retinal pigment epithelium-specific microsomal protein that is post-transcriptionally regulated in vitro, *J. Biol. Chem. 268*, 15751−15757.
15. Jin, M., Li, S., Moghrabi, W. N., Sun, H., and Travis, G. H. (2005) Rpe65 is the retinoid isomerase in bovine retinal pigment epithelium, *Cell 122*, 449−459.
16. Moiseyev, G., Chen, Y., Takahashi, Y., Wu, B. X., and Ma, J. X. (2005) RPE65 is the isomerohydrolase in the retinoid visual cycle, *Proc. Natl. Acad. Sci. U.S.A. 102*, 12413−12418.
17. Redmond, T. M., Yu, S., Lee, E., Bok, D., Hamasaki, D., Chen, N., Goletz, P., Ma, J. X., Crouch, R. K., and Pfeifer, K. (1998) Rpe65 is necessary for production of 11-cis-vitamin A in the retinal visual cycle, *Nat. Genet. 20*, 344−351.
18. Tsilou, E., Hamel, C. P., Yu, S., and Redmond, T. M. (1997) RPE65, the major retinal pigment epithelium microsomal membrane protein, associates with phospholipid liposomes, *Arch. Biochem. Biophys. 346*, 21−27.
19. Bavik, C. O., Busch, C., and Eriksson, U. (1992) Characterization of a plasma retinol-binding protein membrane receptor expressed in the retinal pigment epithelium, *J. Biol. Chem. 267*, 23035−23042.
20. Xue, L., Gollapalli, D. R., Maiti, P., Jahng, W. J., and Rando, R. R. (2004) A palmitoylation switch mechanism in the regulation of the visual cycle, *Cell 117*, 761−771.
21. Kloer, D. P., Ruch, S., Al-Babili, S., Beyer, P., and Schulz, G. E. (2005) The structure of a retinal-forming carotenoid oxygenase, *Science 308*, 267−269.
22. Nicoletti, A., Wong, D. J., Kawase, K., Gibson, L. H., Yang-Feng, T. L., Richards, J. E., and Thompson, D. A. (1995) Molecular characterization of the human gene encoding an abundant 61 kDa protein specific to the retinal pigment epithelium, *Hum. Mol. Genet. 4*, 641−649.
23. Frangioni, J. V., and Neel, B. G. (1993) Solubilization and purification of enzymatically active glutathione S-transferase (pGEX) fusion proteins, *Anal. Biochem. 210*, 179−187.
24. Berge, B., and Renault, A. (1993) Ellipsometry study of 2D crystallization of 1-alcohol monolayers at the water surface, *Europhys. Lett. 21*, 773−777.
25. Venien-Bryan, C., Lenne, P. F., Zakri, C., Renault, A., Brisson, A., Legrand, J. F., and Berge, B. (1998) Characterization of the growth of 2D protein crystals on a lipid monolayer by ellipsometry and rigidity measurements coupled to electron microscopy, *Biophys. J. 74*, 2649−2657.
26. Bavik, C. O., Eriksson, U., Allen, R. A., and Peterson, P. A. (1991) Identification and partial characterization of a retinal pigment epithelial membrane receptor for plasma retinol-binding protein, *J. Biol. Chem. 266*, 14978−14985.
27. Lund, O., Nielsen, M., Lundegaard, C., and Worning, P. (2002) CPHmodels 2.0: X3M a computer program to extract 3D models, CASP5 Conference A102.
28. Pettersen, E. F., Goddard, T. D., Huang, C. C., Couch, G. S., Greenblatt, D. M., Meng, E. C., and Ferrin, T. E. (2004) UCSF Chimera—a visualization system for exploratory research and analysis, *J. Comput. Chem. 25*, 1605−1612.
29. Sanner, M. F., Olson, A. J., and Spehner, J. C. (1996) Reduced surface: an efficient way to compute molecular surfaces, *Biopolymers 38*, 305−320.
30. Ma, J., Zhang, J., Othersen, K. L., Moiseyev, G., Ablonczy, Z., Redmond, T. M., Chen, Y., and Crouch, R. K. (2001) Expression, purification, and MALDI analysis of RPE65, *Invest. Ophthalmol. Visual Sci. 42*, 1429−1435.
31. Mata, N. L., Moghrabi, W. N., Lee, J. S., Bui, T. V., Radu, R. A., Horwitz, J., and Travis, G. H. (2004) Rpe65 is a retinyl ester binding protein that presents insoluble substrate to the isomerase in retinal pigment epithelial cells, *J. Biol. Chem. 279*, 635−643.
32. Jahng, W. J., David, C., Nesnas, N., Nakanishi, K., and Rando, R. R. (2003) A cleavable affinity biotinylating agent reveals a retinoid binding role for RPE65, *Biochemistry 42*, 6159−6168.
33. Zhan, Y., Song, X., and Zhou, G. W. (2001) Structural analysis of regulatory protein domains using GST-fusion proteins, *Gene 281*, 1−9.
34. Kyte, J., and Doolittle, R. F. (1982) A simple method for displaying the hydropathic character of a protein, *J. Mol. Biol. 157*, 105−132.
35. Garnier, J., Gibrat, J. F., and Robson, B. (1996) GOR method for predicting protein secondary structure from amino acid sequence, *Methods Enzymol. 266*, 540−553.
36. Jones, D. T. (1999) Protein secondary structure prediction based on position-specific scoring matrices, *J. Mol. Biol. 292*, 195−202.
37. Cserzo, M., Wallin, E., Simon, I., von Heijne, G., and Elofsson, A. (1997) Prediction of transmembrane alpha-helices in prokaryotic membrane proteins: the dense alignment surface method, *Protein Eng. 10*, 673−676.
38. Pollastri, G., Przybylski, D., Rost, B., and Baldi, P. (2002) Improving the prediction of protein secondary structure in three and eight classes using recurrent neural networks and profiles, *Proteins 47*, 228−235.
39. Ma, J., Xu, L., Othersen, D. K., Redmond, T. M., and Crouch, R. K. (1998) Cloning and localization of RPE65 mRNA in salamander cone photoreceptor cells, *Biochim. Biophys. Acta 1443*, 255−261.
40. Eriks, L. R., Mayor, J. A., and Kaplan, R. S. (2003) A strategy for identification and quantification of detergents frequently used in the purification of membrane proteins, *Anal. Biochem. 323*, 234−241.
41. Clark, E. D. B. (1998) Refolding of recombinant proteins, *Curr. Opin. Biotechnol. 9*, 157−163.
42. Moiseyev, G. P., Chen, Y., Crouch, R. K., and Ma, J. X. (2005) Iron is required for the isomerohydrolase activity in the visual cycle, *Invest. Ophthalmol. Visual Sci*., E-Abstract 1056.

43. Chen, H., and Anderson, R. (1992) Lipids of frog retinal pigment epithelium: comparison with rod outer segments, retina, plasma and red blood cells, *Curr. Eye Res. 11*, 793−800.
44. Lahdo, R., Coillet-Matillon, S., Chauvet, J. P., and de La Fourniere-Bessueille, L. (2002) The amyloid precursor protein interacts with neutral lipids, *Eur. J. Biochem. 269*, 2238−2246.
45. Lahdo, R., and De La Fourniere-Bessueille, L. (2004) Insertion of the amyloid precursor protein into lipid monolayers: effects of cholesterol and apolipoprotein E, *Biochem. J. 382*, 987−994.
46. Kennedy, M. T., Brockman, H., and Rusnak, F. (1997) Determinants of calcineurin binding to model membranes, *Biochemistry 36*, 13579−13585.
47. Guruprasad, K., and Dhamayanthi, P. (2004) Structural plasticity associated with the beta-propeller architecture, *Int. J. Biol. Macromol. 34*, 55−61.
48. Neer, E. J., and Smith, T. F. (1996) G protein heterodimers: new structures propel new questions, *Cell 84*, 175−178.
49. Baker, S. C., Saunders, N. F., Willis, A. C., Ferguson, S. J., Hajdu, J., and Fulop, V. (1997) Cytochrome cd1 structure: unusual haem environments in a nitrite reductase and analysis of factors contributing to beta-propeller folds, *J. Mol. Biol. 269*, 440−455.
50. Fulop, V., and Jones, D. T. (1999) Beta propellers: structural rigidity and functional diversity, *Curr. Opin. Struct. Biol. 9*, 715−721.
51. Renault, A., Lenne, P. F., Zakri, C., Aradian, A., Venien-Bryan, C., and Amblard, F. (1999) Surface-induced polymerization of actin, *Biophys. J. 76*, 1580−1590.
52. Courty, S., Dollet, B., Kassner, K., Renault, A., and Graner, F. (2003) Elasticity and plasticity of two-dimensional amorphous solid layers of beta-lactoglobulin, *Eur. Phys. J. E 11*, 53−59.
53. Niedziela-Majka, A., Rymarczyk, G., Kochman, M., and Ozyhar, A. (1998) GST-induced dimerization of DNA-binding domains alters characteristics of their interaction with DNA, *Protein Expression Purif. 14*, 208−220.
54. Haldeman, M. T., Xia, G., Kasperek, E. M., and Pickart, C. M. (1997) Structure and function of ubiquitin conjugating enzyme E2−25K: the tail is a core-dependent activity element, *Biochemistry 36*, 10526−10537.
55. Bjorndal, B., Trave, G., Hageberg, I., Lillehaug, J. R., and Raae, A. J. (2003) Expression and purification of receptor for activated C-kinase 1 (RACK1), *Protein Expression Purif. 31*, 47−55.
56. Vargo, M. A., Nguyen, L., and Colman, R. F. (2004) Subunit interface residues of glutathione S-transferase A1-1 that are important in the monomer−dimer equilibrium, *Biochemistry 43*, 3327−3335.
57. Driessen, C. A., Winkens, H. J., Hoffmann, K., Kuhlmann, L. D., Janssen, B. P., Van Vugt, A. H., Van Hooser, J. P., Wieringa, B. E., Deutman, A. F., Palczewski, K., Ruether, K., and Janssen, J. J. (2000) Disruption of the 11-cis-retinol dehydrogenase gene leads to accumulation of cis-retinols and cis-retinyl esters, *Mol. Cell. Biol. 20*, 4275−4287.
58. Belyaeva, O. V., Stetsenko, A. V., Nelson, P., and Kedishvili, N. Y. (2003) Properties of short-chain dehydrogenase/reductase RalR1: characterization of purified enzyme, its orientation in the microsomal membrane, and distribution in human tissues and cell lines, *Biochemistry 42*, 14838−14845.
59. Simon, A., Hellman, U., Wernstedt, C., and Eriksson, U. (1995) The retinal pigment epithelial-specific 11-cis retinol dehydrogenase belongs to the family of short chain alcohol dehydrogenases, *J. Biol. Chem. 270*, 1107−1112.
60. Suzuki, Y., Ishiguro, S., and Tamai, M. (1993) Identification and immunohistochemistry of retinol dehydrogenase from bovine retinal pigment epithelium, *Biochim. Biophys. Acta 1163*, 201−208.
61. Simon, A., Romert, A., Gustafson, A. L., McCaffery, J. M., and Eriksson, U. (1999) Intracellular localization and membrane topology of 11-cis retinol dehydrogenase in the retinal pigment epithelium suggest a compartmentalized synthesis of 11-cis retinaldehyde, *J. Cell Sci. 112* (Part 4), 549−558.

BI0519405